Effect of Substrate–Induced Localized Stress on the Combustion Properties of Al/CuO Reactive Multilayer Films

Baptiste Julien, Pascal Dubreuil, Claudie Josse, Ludovic Salvagnac, Sylvain Pelloquin, Alain Estève, Carole Rossi

▶ **To cite this version:**

Baptiste Julien, Pascal Dubreuil, Claudie Josse, Ludovic Salvagnac, Sylvain Pelloquin, et al.. Effect of Substrate–Induced Localized Stress on the Combustion Properties of Al/CuO Reactive Multilayer Films. Thin Solid Films, 2021, 740, pp.139000. 10.1016/j.tsf.2021.139000 . hal-03431059

HAL Id: hal-03431059
https://laas.hal.science/hal-03431059

Submitted on 16 Nov 2021

HAL is a multi-disciplinary open access archive for the deposit and dissemination of scientific research documents, whether they are published or not. The documents may come from teaching and research institutions in France or abroad, or from public or private research centers.

L'archive ouverte pluridisciplinaire **HAL**, est destinée au dépôt et à la diffusion de documents scientifiques de niveau recherche, publiés ou non, émanant des établissements d'enseignement et de recherche français ou étrangers, des laboratoires publics ou privés.

Effect of Substrate–Induced Localized Stress on the Combustion Properties of Al/CuO Reactive Multilayer Films

*Baptiste Julien[1], Pascal Dubreuil[1], Claudie Josse[2], Ludovic Salvagnac[1], Sylvain Pelloquin[1], Alain Esteve[1], Carole Rossi[1]**

[1] LAAS-CNRS, University of Toulouse, 7 Avenue du colonel Roche, 31400 Toulouse, France

[2] Centre de Micro Caractérisation Raymond Castaing (UMS 3623), 3 Rue Caroline Aigle, 31400 Toulouse, France

[*]e-mail : rossi@laas.fr

Keywords: Reactive thin film; Multilayer; Aluminum/cupric oxide; Thermite; Stress; Combustion velocity; Energy electron loss spectroscopy; Plasma-enhanced chemical vapour deposition

Abstract

Reactive multilayer films are a high energy dense configuration for energetics widely studied for various pyrotechnic applications. The objective of this study is to investigate the influence of substrate–induced localized stress on the combustion properties of Al/CuO reactive thin films. Square microbumps are patterned on glass substrates to serve as embedded stressor elements. Stress-induced structural or morphological changes of the materials deposited around the microbumps are characterized using high-magnification transmission and scanning electron microscopy, providing simultaneous nanometer imaging resolution and detailed chemical analysis. The structural and chemical changes (appearance of reactant intermixing and voids) around the microbumps modify the energetic reservoir and the thermophysical properties of the film. The heat of reaction, the flame temperature and the effective thermal conductivity of the film are altered (loss of ~15%), leading to a global decrease in the material reactivity. The flame velocity of the film deposited on the substrate with microbumps drops by 9.2%, 32.4% and

48.7% for microbump heights of 0.15, 0.35 and 0.83 µm, respectively. This work helps deepen the understanding of the effect of stress-induced strain on reactive film combustion properties and provides perspectives for controlling the reaction of reactive thin films by tailoring the strain distributions within the films.

1. Introduction

Among energetic materials, thermite multilayers, also referred to as thermite nanolaminates, are composed of alternating nanolayers (tens to hundreds of nm) of metal and oxidizer. Al/CuO multilayers have attracted considerable interest due to their capability to store and promptly release an important amount of energy (up to 4 $kJ.g^{-1}$) in the sudden emission of light and heat. In recent decades, the magnetron sputtering technique has become a standard manufacturing process for Al/CuO multilayers elaboration [1–5]. Its relatively low cost and ease of use for the fabrication of large-area thin films make it possible to envision transfer to industrial products with applications in microelectromechanical systems [6–9], igniters [3,6–8,10–13], material bonding [14,15] or combustion synthesis [16,17]. While it is recognized that both the sensitivity and combustion regime can be manipulated via layering, reactant spacing and the stoichiometric ratio [18,19], relatively little is known about the effect of residual or substrate–induced localized stress on the combustion performance of Al/CuO reactive thin films. Therefore, the purpose of this work is to investigate how stress-induced strain present in reactive thin films deposited on structured substrates changes the structure and morphology of the layering and, as a direct consequence, affects the combustion properties. For that purpose, we produced 2D arrays of square microbump structures of different heights and spacings. The combustion of Al/CuO multilayers sputter-deposited on these patterned substrates was then characterized. We show that the flame velocity exponentially drops with respect to the microbump height and density. The correlation between the combustion velocity slowdown and the stress-induced strain modification of the morphology and microstructure around the microbump sidewalls is

clearly established using high-resolution electron microscopy. Electron energy loss spectroscopy (EELS) carried out in scanning transmission electronic microscopy (STEM) mode enables us to accurately characterize the structural and chemical modifications (appearance of reactant intermixing and voids) to correlate these morphological changes with the combustion velocity decrease that can reach 50%. This technological work demonstrates that localized stress in the microstructure of reactive multilayers greatly influences their combustion properties. This work also shows that tailoring the strain distributions by patterning the substrate prior to multilayers deposition could be further investigated to control the reaction of Al/CuO thin films without changing the layering of the system itself.

2. Experimental details

2.1. Preparation of glass substrates featuring square microbumps

Glass substrates (alkali-free alumina-borosilicate glass) of 500 µm in thickness, with patterned 5 × 5 µm² square microbumps were prepared using photolithography and dry etching techniques, as briefly summarized in **Figure 1a**. First, a thin film of silicon nitride (SiN_x) was chosen for its low thermal conductivity (~10 $W.m^{-1}.K^{-1}$) and because it is chemically inert with Al/CuO thermite. It was deposited by plasma-enhanced chemical vapor deposition, using flows of SiH_4 (80 sccm), NH_3 (10 sccm) and N_2 (1960 sccm), under a base pressure of 8.6×10^4 Pa. The plasma was generated using 380 kHz low-frequency excitation with a power of 185 W. The silicon nitride film was then patterned using conventional photolithography and etched using an inductively coupled plasma reactive ion etching technique. To achieve this, CF_4 plasma with a power of 485 W (flow rate of 40 sccm) was generated under a base pressure of 600 Pa. In addition, a direct-current voltage bias of 40 V was applied to enhance ions bombardment at the sample surface. Several substrates were thus prepared, using different deposition and etching times to obtain various microbump heights h of 150 nm, 350 nm, 830 nm and 1 µm. While keeping the SiN_x microbump surface area at 5 × 5 µm², various lattice periodicities (p = 10, 15

and 20 µm) were used to change the microbump density per unit area. **Figure 1b** gives a schematic of the microbump lattice. **Figure 1c** shows a matrix of 830 nm thick microbumps arranged with a periodicity of 15 µm (h = 0.83 µm and p = 15 µm), with a magnified image of a single microbump showing the square-like shape and good verticality of the sidewalls. The inclusion volume loading (ratio of microbumps) with respect to the multilayer volume, calculated as detailed in **Figure 1b**, is reported in **Table 1** for each engineered substrate: it ranges from 0.3 to 4.2%.

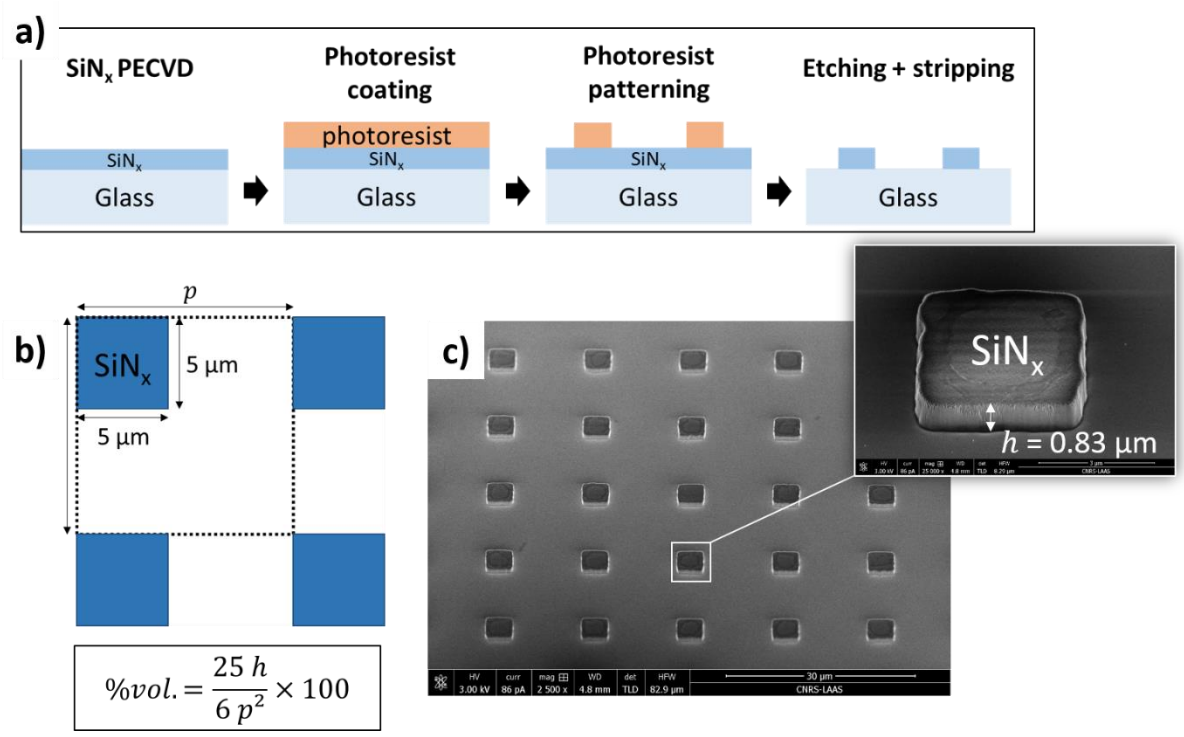

Figure 1. (a) Process flow developed to prepare propagation-test samples with SiN_x microbumps. (b) Schematic of a lattice composed of four microbumps. Each microbump is 25 µm². The inclusion volume loading (%vol.) is calculated as a function of the microbump area (25 µm²), microbump height (h), total Al/CuO multilayer thickness (6 µm), and lattice periodicity (p). (c) SEM images showing a matrix of 830 nm thick SiN_x microbumps, with a periodicity of 15 µm. The magnified image in the inset shows a single microbump.

Table 1. *Summary of sample dimensional features.*

SiN_x microbump height h (µm)	Lattice periodicity p (µm)	Inclusion volume loading (%)
0.15	15	0.28
0.35	15	0.65
0.83	15	1.54
1	20	1.04
1	10	4.17

2.2. Al/CuO multilayer sputter deposition and sample preparation

The reactive multilayers used in this work were deposited using a direct current (DC) magnetron-sputtering system from TFE (Thin Film Equipment, Italy). Al and CuO were sputtered using Cu and Al targets (Neyco, France) consisting in 20 cm by 8 cm 99.99 % purity square sides and 6 mm thick. The base pressure during the deposition is set at 5×10^{-5} Pa. O_2 and Ar gas flow rates of 16 and 32 sccm were used for CuO deposition with a partial pressure of 1 Pa. The Ar partial pressure during Al deposition was maintained at 0.5 Pa. At the end of each bilayer deposition, the sample is cooled at ambient temperature, under vacuum, for 600 s. The Al/CuO bilayer thickness is chosen to be 400 nm, with Al and CuO layer being 200 nm thick each. This corresponds to an equivalent ratio of 2:1 (fuel-rich configuration). For such configuration, the total process time is around 6 hours. Before each Al/CuO multilayer deposition, the thickness of one Al and one CuO layer is always controlled, as a calibration, with a mechanical profilometer. The residual stress of one Al/CuO bilayer measured after deposition is very low, with a measured value of 19 MPa. Increasing the number of bilayers slightly increases the residual stress before stabilizing at approximately 50 MPa for 10 bilayers. This confirms that stress relaxation is achieved during the multistep deposition procedure, alternating cooling and layer growth stages. For this study, sputter-deposited Al/CuO multilayers composed of 15 bilayers (corresponding to a total thickness of 6 µm) were deposited onto 4" glass wafers through a patterned shadow mask. At the end of the process, the wafers are diced, in order to obtain propagation-test samples, consisting in 25 mm × 2 mm nanothermite lines onto a 32 mm × 18 mm glass chip. The first 8 mm of each line had no microbump in order to obtain a reference propagation velocity (**Figure 2a-c**).

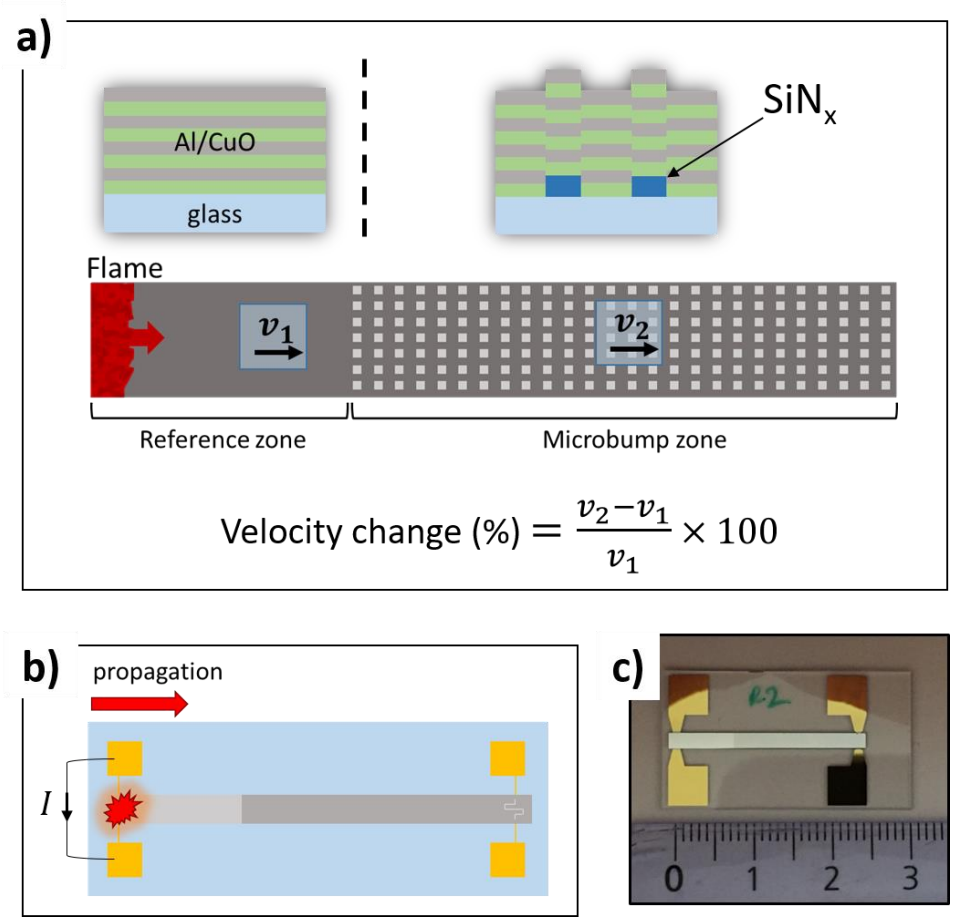

Figure 2. (a) Schematic of the propagation-test sample: Al/CuO multilayer is patterned as a line of 25 mm (length) × 2 mm (width). In the reference zone (left part of the line), the glass substrate is flat, *i.e.*, has no microbumps, which allows measurement of the reference flame velocity (v_1). Schematic (b) and photograph (c) of the propagation-test sample: the self-propagating reaction is ignited through a Ti resistive film on the left side, *i.e.*, in the reference zone.

2.3. Characterization methods

The microstructure of the films was examined using an FEI Helios NanoLab DualBeam scanning electron microscope (SEM). The images were obtained using a backscattered electron detector to achieve good contrast. Transmission electron microscope (TEM) cross-sectional lamellae were prepared using the same equipment. Lamellas were then characterized using STEM on a JEOL JEM-ARM200F cold-FEG instrument operated at 200 kV. Chemical analysis of the microstructure was performed by EELS.

For each sample, the ignition of the Al/CuO multilayers was performed by resistive heating, *i.e.,* by applying a DC current through a Ti resistive filament, previously patterned on the

substrate. The self-propagating reaction was recorded with a high-speed camera (VEO710, Phantom, USA) running at 48000 fps, with a resolution of 512 pixels by 256 pixels. The reaction front was tracked as a function of time to measure the average flame velocity.

3. Results and discussion

3.1. Effect of substrate micropatterning on Al/CuO reactive film combustion properties

The high-speed imaging snapshots presented in **Figure 3a** show the positions of the leading edge combustion front during its propagation for a given propagation-test sample having h = 0.83 µm and p = 15 µm. We observe one distinct linear propagation regime for each region (reference and micropatterned regions). In the reference region, the reaction front propagates at a steady-state velocity of 7.6 ± 0.2 $m.s^{-1}$. In the micropatterned region, the flame slows down to 3.9 ± 0.1 $m.s^{-1}$, corresponding to a decrease of 48.7%. The same behavior is consistently observed for all propagation-test samples. **Figure 3b** and its inset show the evolution of this decrease in velocity as a function of the microbump height (h) and periodicity (p). Keeping p at 15 µm, the flame velocity in the micropatterned region drops by 9.2%, 32.4% and 48.7% for microbump heights of 0.15, 0.35 and 0.83 µm, respectively. Furthermore, the embedded graph shows that decreasing the pitch between microbumps, *i.e.,* increasing the areal density of microbumps, also negatively affects flame propagation (see **Figure 3c**). The relationship between the microbump height and the flame velocity is correlated with the change in flame temperature: grayscale measurements performed within the reaction zone indicate that the reaction front, although its thickness remains roughly constant at ~100 µm, is 20% brighter in the reference region than in the micropatterned region. This indicates that the flame temperature is higher in the latter region. This will be discussed further in section 3.3.

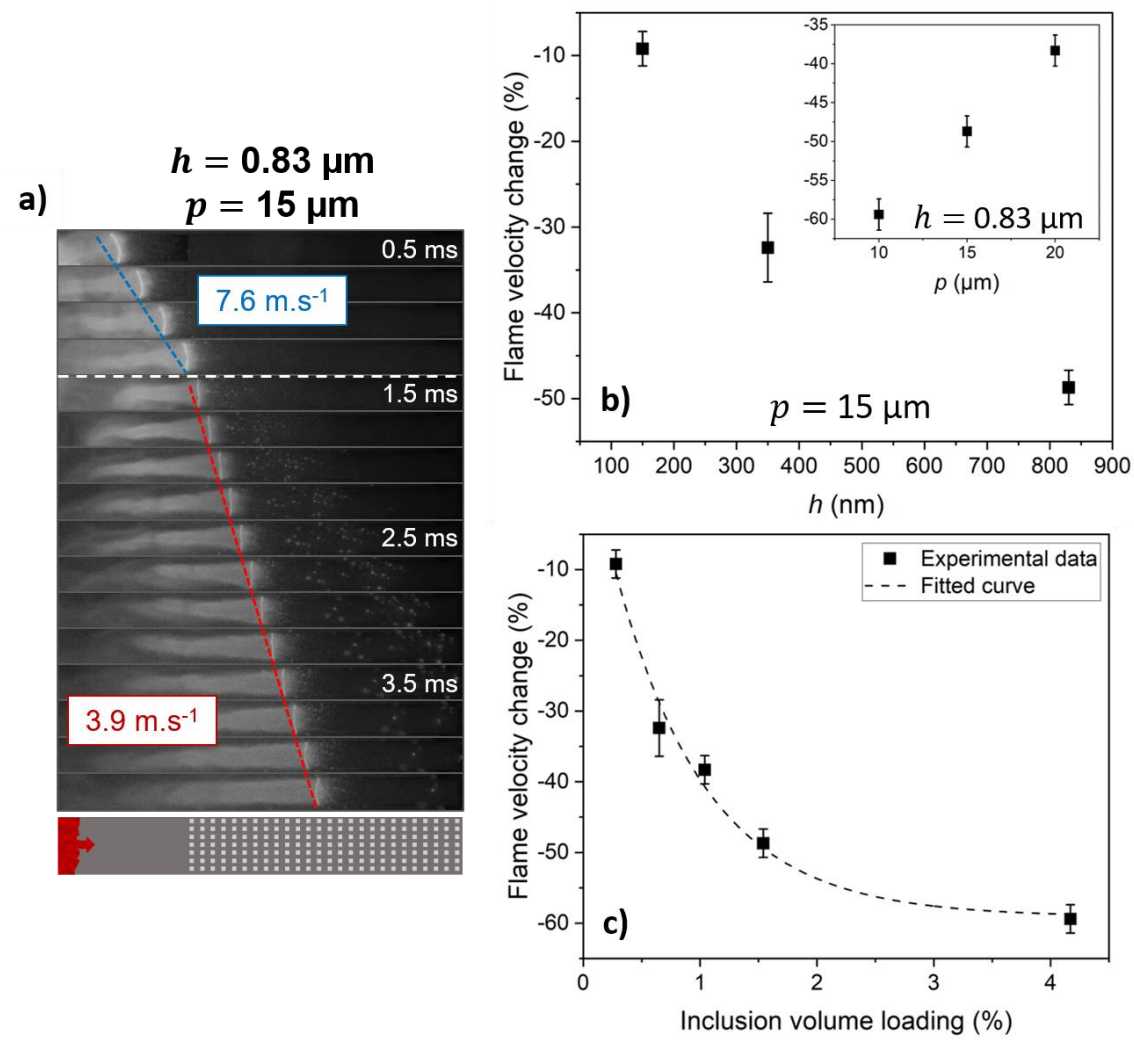

Figure 3. (a) High-speed snapshots showing the reaction front (flame) propagation corresponding to a propagation-test sample with 830 nm thick SiN_x microbumps (p = 15 µm). The white dashed line indicates the frontier separating the reference from the micropatterned regions. (b) Change in the flame velocity as a function of SiN_x microbump height (p = 15 µm). The embedded graph shows the flame velocity change as a function of the lattice periodicity p (h kept at 0.83 µm). (c) Change in the flame velocity as a function of the SiN_x inclusion volume loading, calculated as indicated in **Figure 1b**. The flame velocity is expressed as a change (in %) compared to the reference velocity (v_1), *i.e.*, Al/CuO multilayer deposited on the flat substrate.

The flame velocity of the Al/CuO multilayers clearly decreases exponentially, with a regression coefficient $r^2 = 0.985$, when increasing the inclusion volume loading (**Figure 3c**).

One potential contribution to this slowing down of the flame velocity is the increased heat losses through the substrate due to the addition of a patterned silicon nitride layer, which has a higher thermal diffusivity than glass (α_{SiN_x}= 13 $mm^2.s^{-1}$, α_{glass}= 0.87 $mm^2.s^{-1}$). To test this hypothesis, we produced and characterized additional propagation-test samples (see schematic of samples in **Figure 4a**) in which

- SiN_x microbumps were replaced by Au microbumps (having a high thermal diffusivity, α_{Au} = 127 mm².s^{-1}) with the same dimensions (5 × 5 µm²) and periodicity (p = 15 µm). The reaction front was recorded, and the average velocity (in % change compared to reference Al/CuO multilayers) is plotted versus microbump height in **Figure 4b** (red triangles).
- A thin layer of SiN_x of different thicknesses was deposited on the substrate instead of the microbumps. The flame velocity obtained on nonpatterned SiN_x is compared to that of the reference (**Figure 4b**, blue rhombus).
- Finally, to eliminate any other potential effects caused by the addition of material, glass substrates featuring 300 nm deep blind holes were produced by etching the glass, keeping the same dimensions (5 × 5 µm²) and periodicity (p = 15 µm). The change in the flame velocity is plotted in **Figure 4b** (single green triangle).

Again, all additional propagation-test samples feature a reference region (flat glass substrate) in which a reference velocity is measured. It should be noted that Au microbumps produce the same effect as SiN_x on Al/CuO multilayers combustion: the flame velocity drops when passing through the micropatterned region. Interestingly, while a decade separates the thermal diffusivity of Au from SiNx, their measured velocities show very similar behavior and converge with increasing height: 17.4% deviation at a 140 nm height, dropping to a few % deviation at a 940-nm height. This suggests that the significant ~50% decrease in velocity cannot be attributed only to the modification of diffusivity of the substrate material, which is confirmed by the two other experimentations: Al/CuO multilayer thin film deposited on a SiN_x layer burns at 5.8 ± 0.2 m.s^{-1}, *i.e.* only 12% slower than that deposited on a glass wafer (6.6 ± 0.3 m.s^{-1}), regardless of the thickness of the SiN_x layer. Therefore, the thermal diffusivity modification is totally expressed in the thinner range (~100 nm), and the large decrease in the thicker range is caused by further contributions. This is again confirmed in Al/CuO multilayers deposited on 300-nm-deep blind holes, fitting the results obtained on SiNx microbumps (27.4% decrease in flame velocity) surprisingly well.

Altogether, these experimental results show that the presence of microbumps on the glass substrate affects the propagation of the reaction independently of their thermal diffusivities. To better understand why and how substrate patterning impacts the combustion properties of the Al/CuO film, the microstructure transformation induced by the addition of microbumps prior to the deposition of the reactive layers was analyzed using electron microscopy.

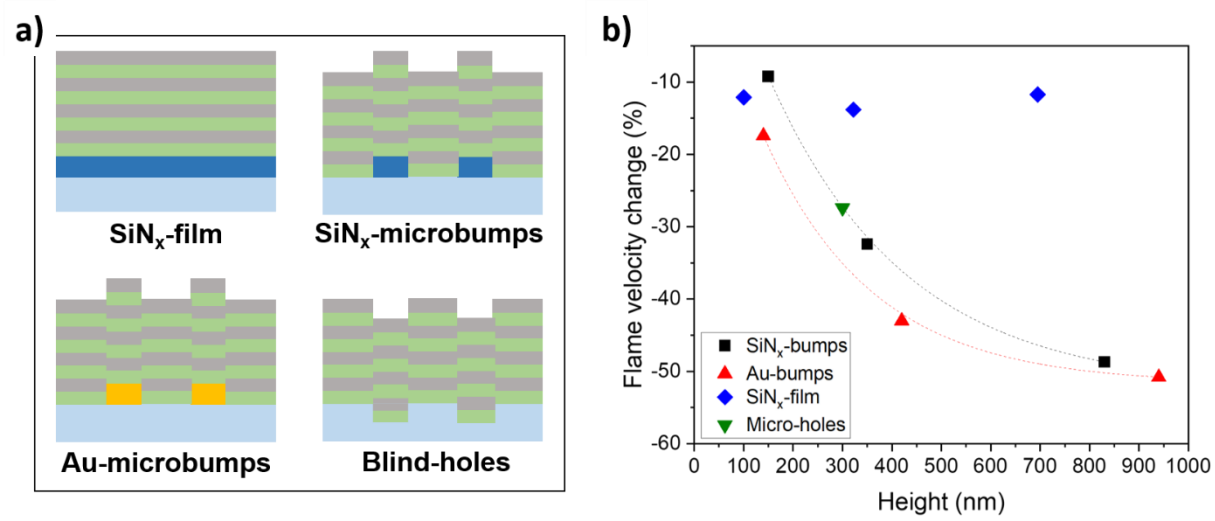

Figure 4. (a) Cross-sectional schematics of the different sample configurations. (b) Flame velocity change of Al/CuO multilayers deposited on the different configurations of substrates described in (a): SiN_x film (blue), Au microbumps (red), SiN_x microbumps (black), and blind microholes (green). Depending on the configuration, the x-axis represents the microbump height, the SiN_x film thickness or the blind-hole depth.

3.2. Effect of substrate micropatterning on the Al/CuO reactive film microstructure

Figure 5 shows cross-sectional SEM images of 15 Al/CuO multilayers deposited onto the two thicker SiN_x microbumps, *i.e.*, h = 350 nm and 830 nm. The presence of microbumps clearly alters the layering and provokes structural modifications: we observe voids around the sidewalls, whereas the layering is well defined on and in the vicinity of the microbumps.

The structural damages and morphological changes are worse for the thickest microbumps (h = 830 nm). Indeed, larger voids are present and extend through the whole multilayer around the microbump sidewalls, while around the 350 nm thick microbumps, only the first four bilayers are damaged. Magnifications of each cross-section confirm the presence of nanovoids around the microbump sidewalls: the voids size is ~20 nm and ~40 nm for 350 nm- and 830 nm-thick microbumps, respectively.

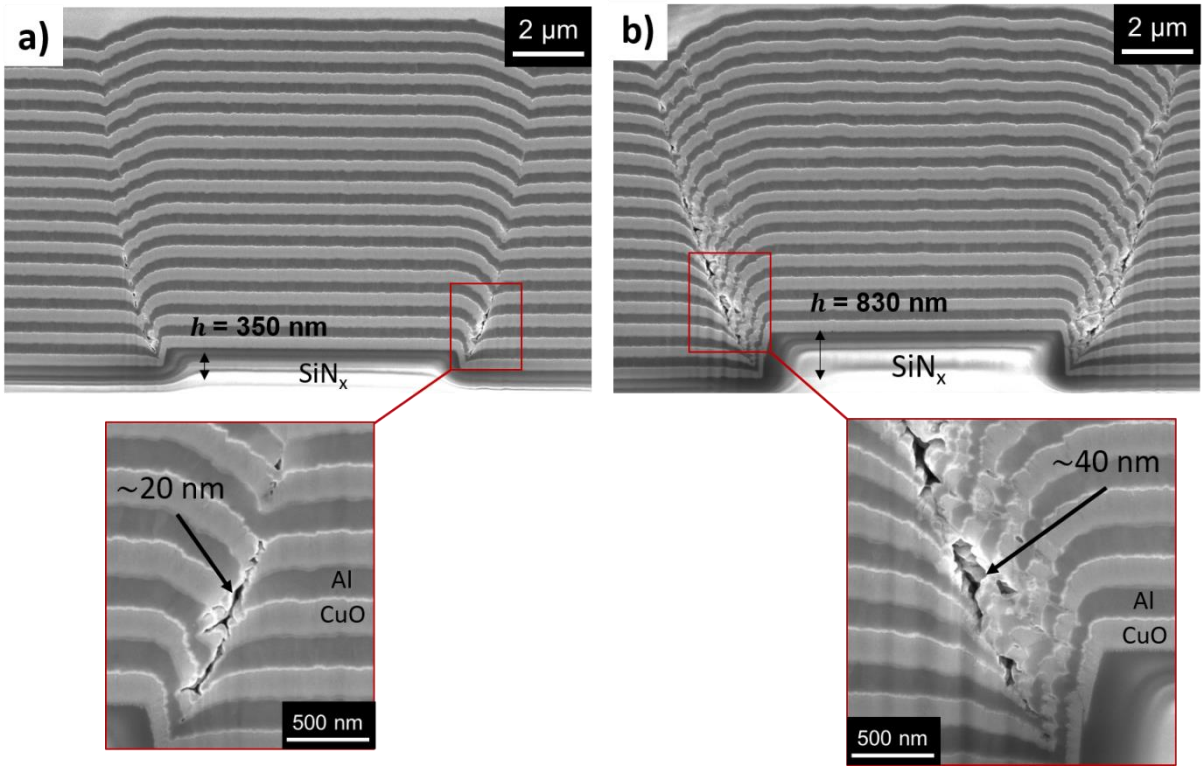

Figure 5. Cross-sectionnal SEM images of Al/CuO multilayers deposited on SiN_x microbumps that are (a) 350 nm and (b) 830 nm thick. Magnified images show details of the damaged areas.

Atomically resolved STEM-HAADF (high-angle annular dark-field imaging) and STEM-EELS were performed in and around the damaged area in the vicinity of the microbumps on propagation-test samples having the thickest SiN_x microbumps. STEM images (**Figure 6**) were taken in a dark field; thus, the darker and brighter regions correspond to Al and CuO compounds, respectively.

Region A – far from the microbump (**Figure 6b**). Electron loss near-edge structure (ELNES) of O-K-edge, Cu-$L_{2,3}$-edges and Al-K edges acquired in the Al/CuO interface support the presence of reactant intermixing, involving CuO_x and AlO_x content. This natural intermixed thin layer with a thickness of ~2-5 nm is caused by atomic interpenetration during the sputtering process [20]. Outside of the interfacial layer, only metallic Al and pure CuO are detected. These features correspond well with those of usual Al/CuO multilayers deposited on perfectly flat surfaces.

Region B – on the microbump sidewalls (**Figure 6c**). In the highly stressed area, *i.e.*, near the voids induced by the microbumps, STEM analyses show that Al/CuO layering is locally tilted (~70°). A thick and distorted layer of 33 ± 8 nm is noticeable at the Al/CuO interface (highlighted by a dashed line). ELNES spectra confirm the intermixing of the three elements (Al, Cu and O) over a scan line that is 40 nm long. From left to right (from the Al to CuO layer), the relative intensity of the Cu-L_3 peak (at 931 eV) increases linearly, which may indicate that the CuO_x-based phase content gradually decreases through the intermixed layer. This tends to indicate that, in this particular region, the natural interdiffusion of Cu and O atoms in the Al layer is highly efficient: the intermixing zone is more than 3 times thicker than the common native alumina interfaces in Al/CuO multilayers, as measured in region A.

The presence of microbumps alters the deposition process around the terrace steps, resulting in tilted layering compared to the layering on the plane substrate, with subsequent deposition of layers in almost perpendicular walls and visible differences when compared to flat and defectless portions (shrinking and image contrast modifications). Additional high-resolution TEM images (not shown) around the microbumps reveal porosity of the polycrystalline structure of the CuO film, which might be one cause of the thicker interfacial layer observed in the same regions, as a defective or porous film is subject to increased atomic interdiffusion during atomic deposition.

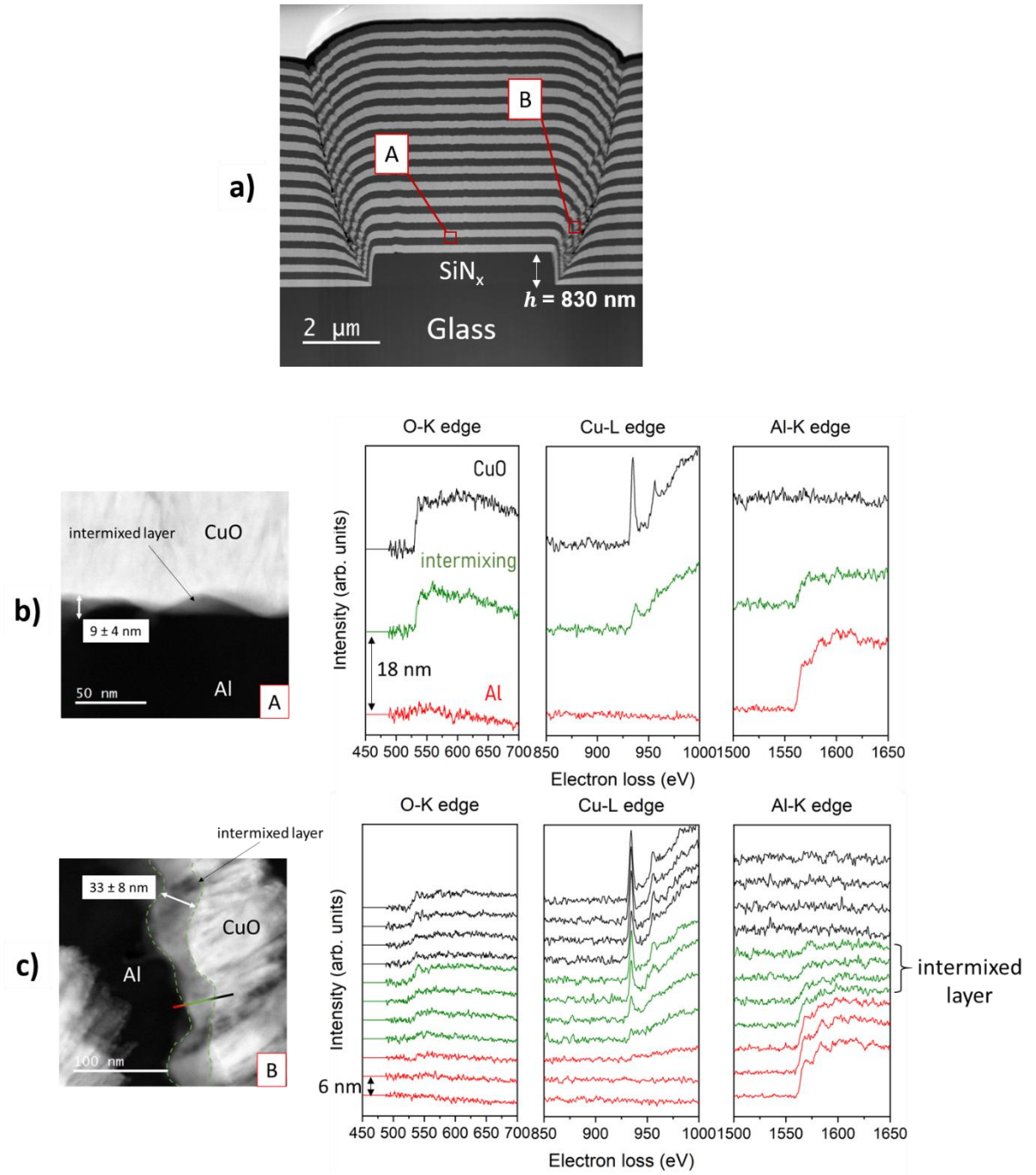

Figure 6. (a) Cross-sectional TEM images showing Al/CuO layering around one SiN_x microbump having a height of 830 nm. A and B correspond to the two regions of interest. (b) and (c) present HAADF-STEM images corresponding to regions A and B. EELS spectra (for Cu-L, O-K and Al-K edges) were acquired across the intermixed layers. The colors in the spectra indicate the different layering domains.

3.3. Correlations between microstructure transformation and combustion properties

Now, considering a purely macroscopic observation in which the Al/CuO multilayers behaves as a "quasihomogenous" system, the reaction front velocity can be calculated using the analytical model (Equation 1) proposed by Armstrong and Koszykowski [21]:

$$v^2 = \frac{3RT_f^2\alpha^2}{\delta'^2 E\left(T_f - T_0\right)} Ae^{-\frac{E}{RT_f}} \quad (1)$$

where T_f and T_0 are the adiabatic (or flame) temperature of the reaction and the initial temperature (298 K), respectively. α is the average thermal diffusivity of the unreacted material, E is an effective activation energy of the limiting reaction step, A is its Arrhenius prefactor, R is the universal gas constant, and δ' is the length of mass diffusion, generally corresponding to 1/4 of the bilayer thickness. Equation (1) clearly shows that the two central parameters controlling the thermite multilayer steady-state propagation velocity are the effective thermal diffusivity of the Al/CuO multilayers, represented by α, and the flame temperature T_f, directly related to the chemistry and heat of reaction.

3.3.1. Thermophysical properties of the Al/CuO multilayers

The average thermal conductivity λ_{ML}, density ρ_{ML} and heat capacity $C_{p,ML}$ of a multilayer system composed of Al and CuO layers are estimated using equation (2), (3) and (4) respectively.

$$\frac{w_{Al} + w_{CuO}}{\lambda_{ML}} = \frac{w_{Al}}{\lambda_{Al}} + \frac{w_{CuO}}{\lambda_{CuO}} \quad (2)$$

$$\rho_{ML} = \frac{\rho_{Al}w_{Al} + \rho_{CuO}w_{CuO}}{w_{Al} + w_{CuO}} \quad (3)$$

$$C_{p,ML} = \frac{C_{p,Al}w_{Al} + C_{p,CuO}w_{CuO}}{w_{Al} + w_{CuO}} \quad (4)$$

where λ_i and ω_i are the thermal conductivities and the thickness of Al and CuO, ρ_i are the densities, and $C_{p,i}$ are the heat capacities, for Al and CuO species. The thermal diffusivity of the system is then calculated as: $\alpha_{ML} = \lambda_{ML}/\rho_{ML}C_{p,ML}$.

The thermophysical properties of Al and CuO and calculated for a 2:1 Al/CuO multilayers ($w_{Al} = w_{CuO} = 200$ nm) are summarized in **Table 2.**

Table 2*. Thermophysical properties of Al, CuO thin films and calculated for a 2:1 Al/CuO multilayers.*

	Al	CuO	2:1 Al/CuO multilayers
Density (kg.m^{-3})	2698	6313	4506
Thermal conductivity (W.m^{-1}.K^{-1})	237	33	58
Heat capacity (J.kg^{-1}.K^{-1})	897	532	715
Thermal diffusivity (m^2.s^{-1})	9.79×10^{-5}	0.98×10^{-5}	1.80×10^{-5}

The theoretical heat of reaction and flame temperature are calculated to be 3.3 kJ.g^{-1}, corresponding to 15% of 3.9 kJ.g^{-1} (theoretical heat of reaction of stoichiometric Al/CuO [22]) and 2417 K (15% less than the adiabatic temperature of the Al/CuO reaction, in stoichiometric conditions). The activation energy E for the Al/CuO multilayers reaction was set to 120 kJ.mol^{-1}, corresponding to the activation energy of oxygen diffusion into amorphous alumina [23]. The constant A was set to 1.22 to fit the steady-state propagation experimental value ($v_1 = 7.6$ m.s^{-1}, **Figure 3a**).

3.3.2. Impact of interface thickening on the flame temperature and thermal diffusivity

To quantify the changes in the multilayers thermophysical properties (λ^*_{ML} *and* α^*_{ML}) and reactional characteristics (ΔH_* *and* T_{f*}), the volume of intermixing regions that are created around the microbumps is equally distributed on the Al/CuO interfaces (**Figure 7**). Assuming that the interfacial region, w_i, acts as a dead layer, it does penalize the energetic reservoir and

consequently the flame temperature T_f. The heat loss decreases due to intermixing can be related to the ratio w_i/δ [24,25]. Furthermore, since T_f is directly proportional to the heat of reaction ΔH, the adiabatic flame temperature can also be estimated following the same relation:

$$\Delta H_* = \Delta H\left(1 - \frac{2w_i}{\delta}\right) \quad and \quad T_{f*} = T_f\left(1 - \frac{2w_i}{\delta}\right) \tag{5}$$

where ΔH represents the theoretical heat of reaction of fuel-rich Al/CuO (3.3 kJ.g^{-1}). w_i is the average thickness of the intermixed region between Al and CuO, and δ is the bilayer thickness ($\delta = 400$ nm). For 830 nm thick microbumps, the estimated flame temperature is 2018 K (*i.e.*, 17% less than the reaction temperature of Al/CuO films deposited on a flat surface). Note that this loss is in good agreement with the decrease in the reaction front brightness measured from high-speed imaging snapshots (**Figure 3**).

The overall effective thermal conductivity λ^*_{ML} of the Al/CuO multilayers featuring damaged interfaces can be estimated following the well-known Equation 6:

$$\frac{\delta}{\lambda^*_{ML}} = \frac{w_{CuO} - w_i}{\lambda_{CuO}} + \frac{w_{Al} - w_i}{\lambda_{Al}} + \frac{2w_i}{\lambda_i} \tag{6}$$

where w_{CuO}, w_{Al}, w_i and $\lambda_{CuO}, \lambda_{Al}, \lambda_i$ are the average thicknesses and effective thermal conductivities of the different layers: CuO, Al and the damaged interface, respectively.

To estimate the thermal conductivity λ_i of the interfacial layers produced by the microbumps (**Figure 7a**), we consider that the interfacial layers are composed of amorphous alumina (featuring a thermal conductivity of 30 W.m^{-1}.K^{-1}), damaged by a fraction of voids (estimated from TEM images at 10 ± 5 vol.%). Therefore, using Maxwell's model predicting the effective thermal conductivity of a bulk material containing multiple spherical voids [26], the thermal conductivity of the damaged interface λ_i is estimated at ≈ 25 ± 3 W.m^{-1}.K^{-1} by Equation 7**.**

$$\lambda_i = \lambda_{Al_2O_3} + \frac{3\lambda_{Al_2O_3}\left(\lambda_{void} - \lambda_{Al_2O_3}\right)}{2\lambda_{Al_2O_3} + \lambda_{void}}\varphi_{void} \quad (7)$$

$\lambda_{Al_2O_3}$ is the thermal conductivity of amorphous alumina (30 W.m^{-1}.K^{-1}) and λ_{void} is the thermal conductivity of voids *i.e.* air (0.01 W.m^{-1}.K^{-1}). The fraction of voids, φ_{void}, is estimated from TEM images to 10 ± 5 %.

As a result, the total effective thermal conductivity λ^*_{ML} of the damaged Al/CuO multilayers, calculated by Equation 6, decreases from 58 W.m^{-1}.K^{-1} to 47 W.m^{-1}.K^{-1} when w_i ranges from 0 to 35 nm. Therefore, the effective thermal diffusivity α^*_{ML} ranges from 1.8×10^{-5} m².s^{-1} to 1.46×10^{-5} m².s^{-1} when w_i ranges from 0 to 35 nm.

Finally, the propagation velocity v calculated from Equation 1 as a function of the damaged interface thickness w_i and related to the microbump height h is plotted in **Figure 7b.** The calculated velocity drops following a smooth exponential relationship with respect to the interface thickness w_i (featuring a regression coefficient r² = 0.9997). To compare this with experimental data, we assume that an Al/CuO multilayers deposited on 830 nm thick microbumps generates a layer of intermixed/damaged compound with an average thickness w_i = 33 ± 8 nm (indicated by the horizontal bars), corresponding to a calculated velocity of 3.2 m.s^{-1}, which fits relatively well with the experimental velocity of 3.9 ± 0.1 m.s^{-1}. For thinner microbumps, it is difficult to estimate an equivalent interfacial layer w_i with enough accuracy, as the intermixing and void presence are much less pronounced and nonuniform over the multilayer thickness. However, according to the microstructure analysis for Al/CuO deposited on 350 nm thick microbumps (**Figure 5b**), the damaged interface thickness can be estimated to be w_i = 10 ± 5 nm, giving a theoretical velocity of 6 m.s^{-1}, whereas the experimental velocity was measured to be 5.1 ± 0.1 m.s^{-1}. As shown in **Figure 7b**, despite the crude nature of our model, good agreement is obtained in the tendency of the flame slowdown (with a disparity of ~15-20%) with the experimental data.

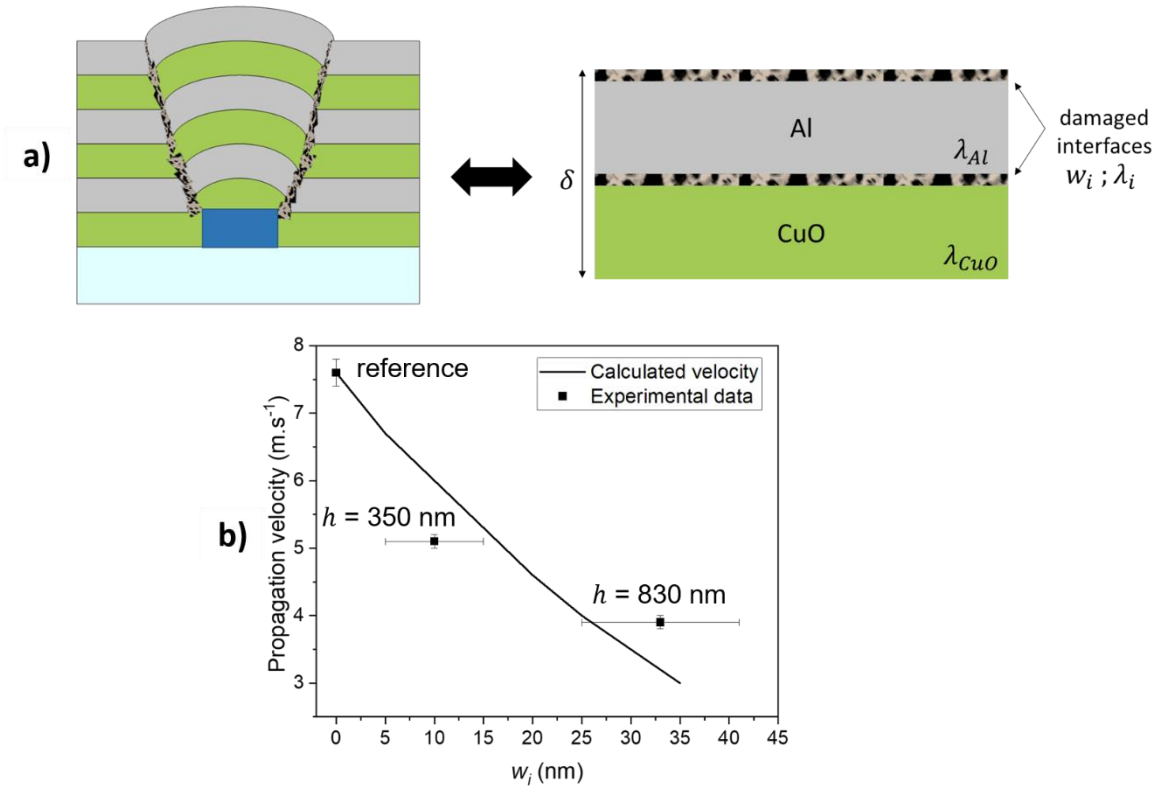

Figure 7. (a) Model of the resulting Al/CuO multilayers structure containing modified regions caused by the micropatterned substrate. (b) Propagation velocity as a function of the damaged interface thickness w_i. Solid-line results from the calculated velocity using Equation (1), whereas squares correspond to experimental data for the reference (no microbumps), h = 350 nm and h = 830 nm. Horizontal error bars represent the incertitude in the estimation of w_i from experimental imaging data.

4. Conclusion

This study investigated the influence of substrate–induced localized stress on the combustion properties of Al/CuO reactive thin films. Square microbumps were patterned on glass substrates to serve as embedded stressor elements. Structural and chemical analyses at the atomic scale level showed that the addition of square microbumps on the substrate (with step heights ranging from 150 nm to ~1 µm) locally stresses the film and affects the layering during the sputtering process. Notably, voids and intermixing regions were detected, particularly when the microbump height was significant. As a direct consequence, the energetic and thermophysical properties of the multilayer film are altered with a direct modification of the burning characteristics: the reaction front velocity drops following an exponential decay relationship with respect to the microbump height or inclusion volume loading. This work demonstrates that tailoring the strain distributions by patterning the substrate prior to multilayers deposition can be an effective way to control the reaction of Al/CuO thin films without changing the layering

of the system itself. Interestingly, this technological approach offers the perspective to deposit in a single sputtering deposition process, *i.e.* on the same substrate, some Al/CuO multilayers having different combustion property just by patterning microbumps on the glass wafer prior to the deposition of the Al/CuO multilayers.

Author contributions

B.J. prepared all samples and performed all characterizations. P.D. and L.S. assisted B.J. in the SiN_x deposition and reactive ion etching process and Al/CuO deposition process, respectively. S.P. also helped in the sample process development. C.J. prepared the lamellae and performed the microscopic observations. A.E. provided some scientific discussions. C.R. provided support in manuscript preparation and supervised the research. The manuscript was written with contributions from all authors. All authors have approved the final version of the manuscript.

Funding sources

C.R. received funding from the European Research Council (ERC) under the European Union's Horizon 2020 research and innovation program (grant agreement No. 832889 - PyroSafe).

Competing financial interests

The authors declare no competing financial interests.

Acknowledgments

The authors thank Teresa Hungria-Hernandez from Centre de Micro Caractérisation R. Castaing (UMS 3623) for her great support with TEM analysis and Tao Wu from LAAS-CNRS for his scientific support. The authors acknowledge support from the European Research Council (H2020 Excellent Science) Researcher Award (grant 832889 – PyroSafe). This work was also supported by the LAAS-CNRS technology platform, a member of the Renatech network.

5. References

[1] E.J. Mily, A. Oni, J.M. Lebeau, Y. Liu, H.J. Brown-Shaklee, J.F. Ihlefeld, J.-P. Maria, The role of terminal oxide structure and properties in nanothermite reactions, THIN SOLID FILMS. 562 (2014) 405–410. https://doi.org/10.1016/j.tsf.2014.05.005.

[2] K.J. Blobaum, M.E. Reiss, J.M. Plitzko, T.P. Weihs, Deposition and characterization of a self-propagating CuOx/Al thermite reaction in a multilayer foil geometry, Journal of Applied Physics. 94 (2003) 2915–2922. https://doi.org/10.1063/1.1598296.
[3] A. Nicollet, G. Lahiner, A. Belisario, S. Souleille, M. Djafari-Rouhani, A. Estève, C. Rossi, Investigation of Al/CuO multilayered thermite ignition, Journal of Applied Physics. 121 (2017) 034503. https://doi.org/10.1063/1.4974288.
[4] M. Petrantoni, C. Rossi, L. Salvagnac, V. Conédéra, A. Estève, C. Tenailleau, P. Alphonse, Y.J. Chabal, Multilayered Al/CuO thermite formation by reactive magnetron sputtering: Nano versus micro, Journal of Applied Physics. 108 (2010) 084323. https://doi.org/10.1063/1.3498821.
[5] D.P. Adams, Reactive multilayers fabricated by vapor deposition: A critical review, Thin Solid Films. 576 (2015) 98–128. https://doi.org/10.1016/j.tsf.2014.09.042.
[6] A. Nicollet, L. Salvagnac, V. Baijot, A. Estève, C. Rossi, Fast circuit breaker based on integration of Al/CuO nanothermites, Sensors and Actuators A: Physical. 273 (2018) 249–255. https://doi.org/10.1016/j.sna.2018.02.044.
[7] L. Glavier, A. Nicollet, F. Jouot, B. Martin, J. Barberon, L. Renaud, C. Rossi, Nanothermite/RDX-Based Miniature Device for Impact Ignition of High Explosives, Propellants, Explosives, Pyrotechnics. 42 (2017) 308–317. https://doi.org/10.1002/prep.201600154.
[8] G. Taton, D. Lagrange, V. Conedera, L. Renaud, C. Rossi, Micro-chip initiator realized by integrating Al/CuO multilayer nanothermite on polymeric membrane, J. Micromech. Microeng. 23 (2013) 105009. https://doi.org/10.1088/0960-1317/23/10/105009.
[9] G.A.A. Rodríguez, S. Suhard, C. Rossi, D. Estève, P. Fau, S. Sabo-Etienne, A.F. Mingotaud, M. Mauzac, B. Chaudret, A microactuator based on the decomposition of an energetic material for disposable lab-on-chip applications: fabrication and test, J. Micromech. Microeng. 19 (2008) 015006. https://doi.org/10.1088/0960-1317/19/1/015006.
[10] P. Zhu, R. Shen, Y. Ye, X. Zhou, Y. Hu, Energetic igniters realized by integrating Al/CuO reactive multilayer films with Cr films, Journal of Applied Physics. 110 (2011) 074513. https://doi.org/10.1063/1.3646489.
[11] X. Zhou, R. Shen, Y. Ye, P. Zhu, Y. Hu, L. Wu, Influence of Al/CuO reactive multilayer films additives on exploding foil initiator, Journal of Applied Physics. 110 (2011) 094505. https://doi.org/10.1063/1.3658617.
[12] S. Fu, R. Shen, P. Zhu, Y. Ye, Metal–interlayer–metal structured initiator containing Al/CuO reactive multilayer films that exhibits improved ignition properties, Sensors and Actuators A: Physical. 292 (2019) 198–204. https://doi.org/10.1016/j.sna.2019.04.019.
[13] J. Xu, Y. Tai, Y. Shen, J. Dai, W. Xu, Y. Ye, R. Shen, Y. Hu, Characteristics of energetic semiconductor bridge initiator based on different stoichiometric ratios of Al/MoO3 reactive multilayer films under capacitor discharge conditions, Sensors and Actuators A: Physical. 296 (2019) 241–248. https://doi.org/10.1016/j.sna.2019.07.015.
[14] A.H. Kinsey, K. Slusarski, S. Sosa, T.P. Weihs, Gas Suppression via Copper Interlayers in Magnetron Sputtered Al–Cu2O Multilayers, ACS Appl. Mater. Interfaces. 9 (2017) 22026–22036. https://doi.org/10.1021/acsami.7b03071.
[15] Jianglong. Yi, Y. Zhang, X. Wang, C. Dong, H. Hu, Characterization of Al/Ti Nano Multilayer as a Jointing Material at the Interface between Cu and Al_2O_3, Mater. Trans. 57 (2016) 1494–1497. https://doi.org/10.2320/matertrans.M2016126.
[16] A. Makino, Heterogeneous flame propagation in the self-propagating, high-temperature, synthesis (SHS) process in multi-layer foils: theory and experimental comparisons, Combustion and Flame. 134 (2003) 273–288. https://doi.org/10.1016/S0010-2180(03)00090-7.

[17] T.S. Dyer, Z.A. Munir, V. Ruth, The combustion synthesis of multilayer NiAl systems, Scripta Metallurgica et Materialia. 30 (1994) 1281-1286. https://doi.org/10.1016/0956-716X(94)90259-3.
[18] J. Zapata, A. Nicollet, B. Julien, G. Lahiner, A. Esteve, C. Rossi, Self-propagating combustion of sputter-deposited Al/CuO nanolaminates, Combustion and Flame. 205 (2019) 389–396. https://doi.org/10.1016/j.combustflame.2019.04.031.
[19] W. Guo, S. Chang, J. Cao, L. Wu, R. Shen, Y. Ye, Precisely Controlled Reactive Multilayer Films with Excellent Energy Release Property for Laser-Induced Ignition, Nanoscale Res Lett. 14 (2019) 301. https://doi.org/10.1186/s11671-019-3124-6.
[20] I. Abdallah, J. Zapata, G. Lahiner, B. Warot-Fonrose, J. Cure, Y. Chabal, A. Esteve, C. Rossi, Structure and Chemical Characterization at the Atomic Level of Reactions in Al/CuO Multilayers, ACS Appl. Energy Mater. 1 (2018) 1762–1770. https://doi.org/10.1021/acsaem.8b00296.
[21] R. Armstrong, Theoretical models for the combustion of alloyable materials, Metall Mater Trans A. 23 (1992) 2339–2347. https://doi.org/10.1007/BF02658035.
[22] S.H. Fischer, M.C. Grubelich, Theoretical energy release of thermites, intermetallics, and combustible metals, Sandia National Labs., Albuquerque, NM (US), SAND-98-1176C; CONF-980728- (1998). https://doi.org/10.2172/6582088.
[23] T. Nabatame, T. Yasuda, M. Nishizawa, M. Ikeda, T. Horikawa, A. Toriumi, Comparative Studies on Oxygen Diffusion Coefficients for Amorphous and γ-Al2O3 Films using 18O Isotope, Jpn. J. Appl. Phys. 42 (2003) 7205. https://doi.org/10.1143/JJAP.42.7205.
[24] T.P. Weihs, T.W. Barbee, M.A. Wall, A low-temperature technique for measuring enthalpies of formation, J. Mater. Res. 11 (1996) 1403–1409. https://doi.org/10.1557/JMR.1996.0176.
[25] A.J. Gavens, D. Van Heerden, A.B. Mann, M.E. Reiss, T.P. Weihs, Effect of intermixing on self-propagating exothermic reactions in Al/Ni nanolaminate foils, Journal of Applied Physics. 87 (2000) 1255–1263. https://doi.org/10.1063/1.372005.
[26] K.B. Kiradjiev, S.A. Halvorsen, R.A. Van Gorder, S.D. Howison, Maxwell-type models for the effective thermal conductivity of a porous material with radiative transfer in the voids, International Journal of Thermal Sciences. 145 (2019) 106009. https://doi.org/10.1016/j.ijthermalsci.2019.106009.